Structure *14*, 1577–1586, October 2006 DOI 10.1016/j.str.2006.08.013

Pheromone Discrimination by the Pheromone-Binding Protein of *Bombyx mori*

Frauke Gräter,[1] Wei Xu,[2] Walter Leal,[2] and Helmut Grubmüller[1,*]
[1] Department of Theoretical and Computational Biophysics
Max-Planck-Institute for Biophysical Chemistry
Am Fassberg 11
37077 Göttingen
Germany
[2] Maeda-Duffey Lab
Department of Entomology
University of California, Davis
Davis, California 95616

Summary

Pheromone-binding proteins are postulated to contribute to the exquisite specificity of the insect's olfactory system, acting as a filter by preferentially binding only one of the components of the natural pheromone. Here, we investigated the possible discrimination of the two very similar components of the natural pheromone gland from the silk moth, *Bombyx mori*, bombykol and bombykal, by the only pheromone-binding protein (BmorPBP) known to be expressed in the pheromone-detecting sensilla. Free-energy calculations and virtual docking indicate that both bombykol and bombykal bind to BmorPBP with similar affinity. In addition, in vitro competitive binding assays showed that both bombykol and bombykal were bound by BmorPBP with nearly the same high affinity. While BmorPBP might filter out other physiologically irrelevant compounds hitting the sensillar lymph, discrimination between the natural pheromone compounds must be achieved by molecular interactions with their cognate receptors.

Introduction

Chemical communication requires the detection of specific olfactory stimuli and their translation into nerve impulses. How olfactory systems achieve the astonishing capacity to discriminate between the broad variety of chemical compounds in the air remains puzzling. As specificity is concerned, the olfactory system of insects evolved for the sexual communication via pheromones as one of the most sophisticated biosensors and has consequently been a subject of intense investigations (Krieger and Breer, 1999; Rutzler and Zwiebel, 2005). There is growing evidence for the notion of a two-step filter in which specific detection of pheromone is mediated by both pheromone-binding proteins (PBPs) and pheromone receptors (Prestwich et al., 1995; Steinbrecht, 1996; Leal, 2005). According to this scenario, it is the combined PBP and receptor specificity that, in two sequential steps, yields the ultra-high selectivity of olfactory receptor cells.

*Correspondence: hgrubmu@gwdg.de

PBPs are located in the sensillar lymph surrounding the olfactory neuron cells. They solubilize the hydrophobic pheromones and deliver them to the receptor resulting in neuronal response, thereby protecting them from degradation and membrane insertion (Vogt and Riddiford, 1981; Steinbrecht et al., 1995). Besides the established role as a passive carrier, the involvement of PBPs in odorant discrimination and perhaps also in receptor activation was suggested (Pophof, 2004; Kaissling, 2001; Rutzler and Zwiebel, 2005). This could explain the coexpression of more than one PBP (and odorant-binding protein in general) in insects within a single sensillum (Steinbrecht, 1996; Maida et al., 1997; Hekmat-Scafe et al., 1997), the biological function of which is otherwise difficult to explain. The coincidence of the number of PBPs with the number of pheromones and olfactory receptors in two silk moth species further corroborates the assumption of the selective transport of only one pheromone by each of the PBPs of one species (Maida et al., 2000). The long-standing speculation that pheromone-PBP complexes might be involved in olfactory receptor activation by directly interacting with the extracellular part of the receptor also requires a high degree of ligand selectivity of PBPs (Du and Prestwich, 1995; Pophof, 2002, 2004).

Quantitative insight into the discriminatory capacity of PBPs between similar molecules, as required for the putative prefiltering and receptor-activating function, can in principle be obtained from the direct measurement of their binding selectivity.

Binding assays showed considerable differences in binding affinities of the PBPs from *Antheraea polyphemus* and *Antheraea pernyi* (Kaissling et al., 1985; Du and Prestwich, 1995; Maida et al., 2000, 2003; Bette et al., 2002), *Lymantria dispar* (Plettner et al., 2000), *Mamestra brassicae* (Maibeche-Coisne et al., 1997), and the silkworm moth *Bombyx mori* (Oldham et al., 2000, 2001) for odorants with only minor differences in the length of the hydrophobic chain, in the chain stereochemistry, or in the oxidative state of the polar head. On the basis of PBP structures and mutation patterns, specific residues within the cavity were suggested to recognize the nature of the polar head and the chain length (Mohanty et al., 2004). Comparative fluorescence binding assays, in contrast, showed only marginal selectivities of PBPs from *Antheraea polyphemus* and *Mamestra brassicae* for fairly different compounds (Campanacci et al., 2001). Similarly, the main pheromone-binding protein from the wild silk moth, *Antheraea polyphemus*, ApolPBP1, shows apparent high affinities to the three constituents of the female-produced sex pheromones: (E,Z)-6,11-hexadecadienyl acetate (E6,Z11-16Ac), (E,Z)-6,11-hexadecadienal (E6,Z11-16Ald), and (E,Z)-4,9-tetradecadienyl acetate (E4,Z9-14Ac) (Leal et al., 2005a). However, ApolPBP1 shows considerable preference for the major constituent, E6,Z11-16Ac, shows lower affinity for the shorter acetate, E4,Z9-14Ac, and no affinity for the aldehyde, E6,Z11-16Ald, when the protein is encountered with equal amounts of the three sex pheromones.

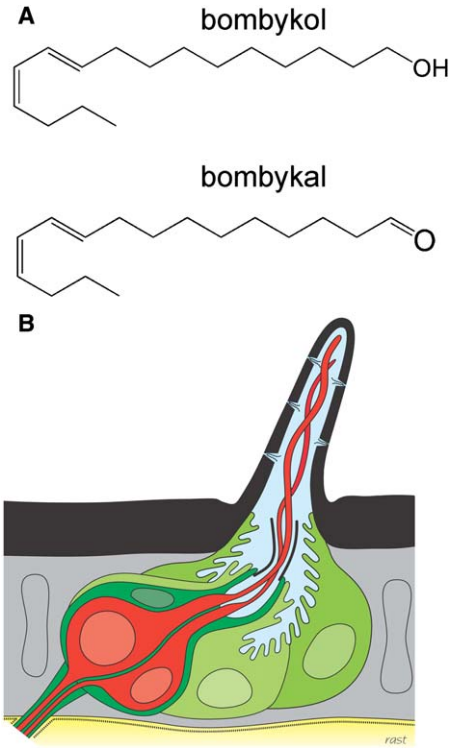

Figure 1. Pheromone Detection in *Bombyx mori*

(A) Schematic drawing of bombykol and bombykal, the two components of the *Bombyx mori* pheromone blend.

(B) Schematic drawing of an olfactory hair of a moth antenna (kindly provided by R.A. Steinbrecht). The two neuron cells of one hair (red) specifically respond to one of the pheromone components. Blue, sensillar lymph; black, cuticle with pores for pheromone entrance.

We here tested this apparent dichotomy by examining the ligand specificity for the PBP of the silkworm moth *Bombyx mori* (BmorPBP). The pheromone gland of *Bombyx mori* secretes two components, bombykol, and its oxidized form, the aldehyde bombykal (Kaissling and Kasang, 1978) (Figure 1A). The slight difference of the two pheromones, a hydroxyl versus a carbonyl head group, results in a strikingly different physiological response. Only bombykol yields mating behavior, whereas bombykal is a behavioral antagonist. This renders *Bombyx mori* an interesting model system to elucidate the mechanism underlying specificity of olfactory systems in general.

Each olfactory hair consists of two olfactory cells, each of which detects one of the two pheromones (Figure 1B). These cells mutually exclusively express two different ORs, which specifically respond to either bombykol or bombykal (Sakurai et al., 2004; Nakagawa et al., 2005). Remarkably, only one type of BmorPBP so far has been found in the sensillar lymph shared by the cells, which shows a high affinity for bombykol (K_D = 105 nM) (Leal et al., 2005b) at physiological pH. The question arises if BmorPBP functions as a filter by being specifically tailored for bombykol and coexpressed with a yet-unknown second BmorPBP as the carrier for bombykal or, alternatively, if BmorPBP is nonspecific and serves as a carrier for both pheromones.

Electrophysiological studies suggest BmorPBP not to bind bombykal in a physiologically active way and thus to assist the olfactory receptors in discriminating between bombykol and bombykal (Pophof, 2004). A previous quantum mechanical study of bombykol-BmorPBP binding suggested specific hydrophobic interactions as responsible for the highly discriminative power of BmorPBP (Klusak et al., 2003). However, this study was restricted to the static crystal structure, hence omitting entropic contributions to the binding free energy and, in particular, the hydrophobic effect.

Here, we aim at quantifying the specificity of BmorPBP to test the hypothesis that BmorPBP is part of a two-layer filter. To this end, we characterize and compare the dynamics and protein-ligand interactions of BmorPBP complexed with bombykol and bombykal by molecular dynamics (MD) simulations. As a direct measure for binding specificity, their difference in binding free energy is calculated by means of free energy perturbation (FEP) (Bash et al., 1987; Simonson et al., 2002). Most surprisingly, only minor differences are seen between the two ligands. This result casts into doubt the assumption of BmorPBP being tailored to only deliver bombykol but not bombykal to the olfactory receptor. The unexpected finding from simulations and additional docking studies prompted us to finally set out to experimentally compare the binding affinities of BmorPBP for bombykol and bombykal by using a newly developed binding assay (Leal et al., 2005b). As reported here, both virtual and empirical binding studies suggest that BmorPBP per se can not discriminate bombykal from bombykol. As far as these two physiologically relevant ligands are concerned, discrimination is likely achieved at the ligand-receptor interactions.

Results and Discussion

Equilibrium Dynamics of the Complexes

The question to what extent PBPs contribute to the selectivity in pheromone reception was addressed by comparing the binding dynamics and energetics of the bombykol and bombykal-BmorPBP complexes. For a better understanding of the ligand-binding properties of BmorPBP, the bombykol-BmorPBP dynamics in the bound state were characterized. Figure 2A quantifies the fluctuations during the free dynamics of the protein backbone and bombykol compared to experimental temperature factors from X-ray scattering (Sandler et al., 2000). As expected, the helical segments, especially when linked via disulphide bonds, show only little fluctuations. Regions of particularly high flexibility (shaded in gray) are the terminal residues 1–24 and 125–137, even though the N-terminal fragment is α helical and contains one of the disulphide bonds. In addition, the histidine-rich loop (residues 60–68) and the loop proximal to it (residues 99–106) are remarkably mobile. This agrees well with the experimental temperature factors (dashed line), which were also found to be high in these regions. The correlation coefficient between the fluctuations from simulation and the temperature factors is 0.5. Overall, the equilibrium protein dynamics fit into the picture of a rigid scaffold as suggested by the available experimental BmorPBP structures.

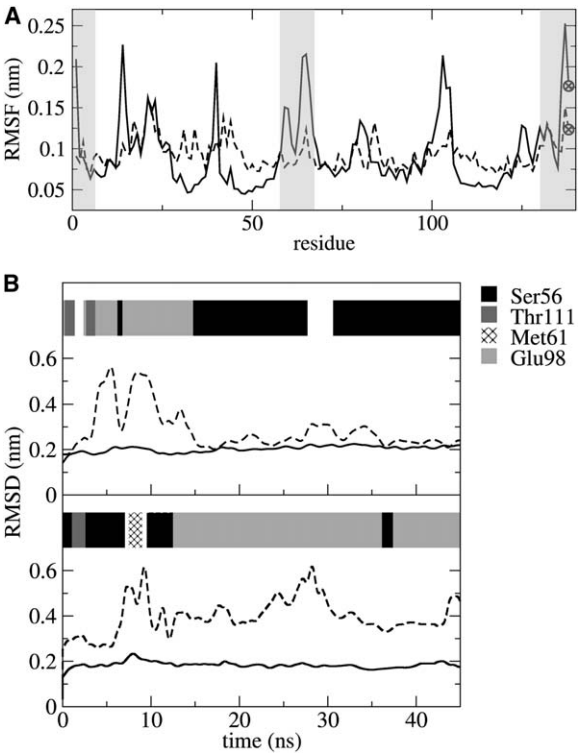

Figure 2. Bombykol-BmorPBP Dynamics

(A) Rms fluctuations of PBP (solid curve) and bombykol (crosses) during the final 40 ns of equilibration in comparison to the temperature factors of 1DQE, after conversion to fluctuations (Wlodek et al., 1997) (dashed). Gray areas indicate regions along which ligand binding and release might occur (terminal fractions and lid).

(B) Rmsd of the protein backbone atoms (solid curves) and bombykol (dashed) from the crystal structure during two molecular dynamics simulations. Major bombykol-PBP hydrogen bonds are indicated. Results from two independent MD simulations with parameters p1 (MD1, top) and p2 (MD2, bottom) are shown.

As indicated in Figure 2A, bombykol with a root-mean-square fluctuation (rmsf) of 0.17 nm showed strikingly large fluctuations, though apparently encapsulated in the cavity. This finding, too, is in agreement with the X-ray experiment, which gives significantly larger crystallographic temperature factors for bombykol compared to the average temperature factor. The nature of this mobility is detailed in Figures 2B. During the two independent MD simulations with different bombykol parameters for the π-system, p1 and p2, the native bombykol-Ser56 hydrogen bond was transiently and reversibly broken and substituted by bonds to other side chains, such as Glu98, Met61, and Thr111. This involved dislocation of the hydrophobic part of bombykol as well, as reflected by the observed high root-mean-square deviation (rmsd) from the crystal structure (dashed lines in Figure 2B). Figure 3A shows the location of the hydrogen-bonding partners for bombykol.

The high mobility of bombykol is also reflected by the numerous hydrophobic contacts formed by the C_{14}-chain of bombykol to BmorPBP during the MD, as depicted in Figure 3B. Many residues of the binding pocket (shown as yellow spheres), which are highly conserved across general OBPs and PBPs (Sandler et al., 2000), were found to significantly contribute to the total Lennard-Jones (LJ) interaction between protein and ligand. The interaction energies between the ligand and the individual residues typically showed high fluctuations. In the half-dissociated conformation of bombykol with a hydrogen bond to Glu98, e.g., Val114, located near the front loop, compensated the loss of interaction at the end of bombykol (to residues Leu8 and Leu90), thereby stabilizing the half-dissociated state. With such a high variability and heterogeneity in the ligand polar and nonpolar interaction network, bombykol can favorably bind to BmorPBP in significantly different conformations, implying a considerable entropic component to the binding free energy. This suggests that also changes in the polar head group, the position and stereochemistry of the double bonds, or the chain length do not have per se to result in a complete loss of binding affinity.

The conventional MD simulation described so far also served as a test of the bombykol force-field parameters. The experimentally determined structure was reproduced during large parts of the MD simulations, with reversible hydrogen-bond rupture and formation. The observation of a highly flexible ligand in the rigid pocket of BmorPBP was robust with regard to the ligand force field used (compare Figure 2B). For the subsequent simulations, set p1 was used.

The two components of the pheromone gland, bombykol and bombykal, differ only in their polar head (Figure 1A). In contrast to bombykol, the carbonyl group of bombykal can interact only as hydrogen bond acceptor with BmorPBP, which excludes anionic side chains such as Glu98 from interacting with bombykal. Do the polar interactions of bombykal, and consequently also its binding mode and position in the pocket, for this reason differ from bombykol? Figure 4 shows the rmsd and hydrogen-bond partners of bombykal during free molecular dynamics simulations, starting from two different

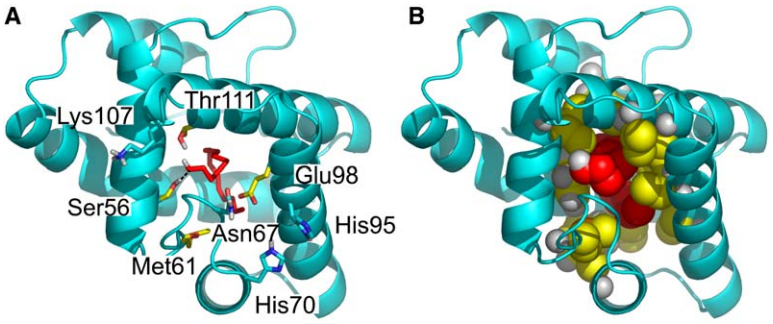

Figure 3. Bombykol in the Hydrophobic Cavity of BmorPBP

(A) Residues forming hydrogen bonds with bombykol (yellow) or bombykal (cyan) are shown as sticks. The hydrogen bond to Ser56 observed in the crystal structure is indicated (black dashed line).

(B) Residues with significant contributions to the hydrophobic interaction energy (>5 kJ/mol) of the protein to bombykol and bombykal are shown as yellow spheres.

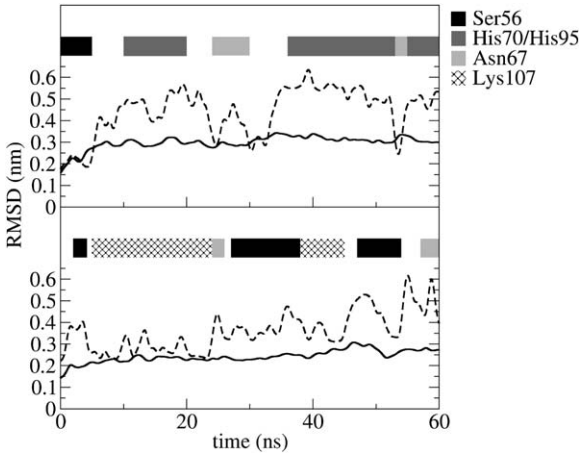

Figure 4. Bombykal-BmorPBP Dynamics

Rmsd of the protein backbone atoms (solid curve) and bombykal (dashed) from the bombykol-BmorPBP crystal structure during two molecular dynamics simulations starting from different ligand conformations (top, MD3; bottom, MD4). Hydrogen bonds of bombykal to four residues of the binding pocket are indicated as gray bars.

equilibrated BmorPBP-bomykol structures with a Ser56-bombykol hydrogen bond. Both simulations show a stable protein structure (solid) and for the ligand (dashed) significant deviations from the Ser56-bound initial structure, which are similar in magnitude and fluctuations to those observed for BmorPBP-bombykol (Figure 2B). Bombykal reversibly forms and breaks hydrogen bonds to Ser56, as bombykol does, but also to His70, His95, Asn67, and Lys107. Thus, bombykal is able to form polar interactions with BmorPBP during major parts of the free dynamics, albeit via formation of hydrogen bonds to other side chains due to the different chemical preference of the carbonyl group. As a consequence of the similar ligand position within the cavity, hydrophobic protein interactions were found to be similar for bombykol and bombykal.

Bombykal versus Bombykol-Binding Free Energies

The results from the equilibrium dynamics indicate similar binding modes of bombykol and bombykal in the cavity of BmorPBP. Since bombykal only functions as a hydrogen-bond acceptor, less favorable bombykal-BmorPBP interactions are expected. This, however, also holds true for the ligand-water interactions in the unbound state, which probably compensates for the observed difference in the bound state.

To quantitatively assess the difference in binding affinity, and to reveal such possible compensation, free-energy perturbation calculations were performed (Figure 5). In these simulations, bombykol in the bound and unbound states was slowly converted into bombykal, as described in Experimental Procedures. According to the thermodynamic cycle shown in Figure 5A, the associated free-energy changes ΔG_{FEP}(prot) and ΔG_{FEP}(aq) yield the difference in binding free energies, $\Delta\Delta G_b$, which are given in Figure 5B. Simulations of bombykol perturbed to bombykal (and vice versa) in the unbound state gave a free-energy change ΔG_{FEP}(aq)

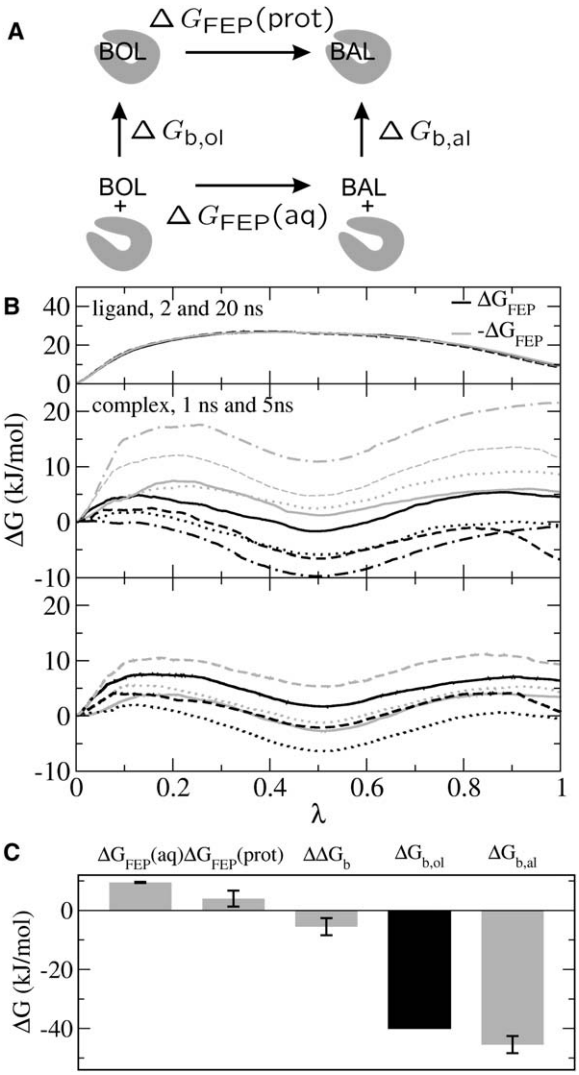

Figure 5. Calculation of the Relative Binding Free Energy of Bombykol and Bombykal to BmorPBP

(A) Thermodynamic cycle (see Experimental Procedures). The relative binding free energy is calculated from $\Delta\Delta G_b = \Delta G_{b,al} - \Delta G_{b,al} = \Delta G_{FEP}(prot) - \Delta G_{FEP}(aq)$.

(B) Free energy change upon "mutating" bombykol to bombykal (black) and back (gray) as obtained from FEP calculations. Results for the simulations of the ligand in water (upper panel) and the ligand bound to the protein (central and lower panel, for 1 ns and 5 ns simulation length, respectively) are shown. Different line styles refer to FEP simulations starting from different conformations of the complex, with identical line styles referring to the same cycle of forward and backward simulation.

(C) Calculated free-energy changes (gray) as obtained from FEP simulations shown in (B) and the resulting binding free energy of bombykal with respect to the experimental binding free energy of bombykol (black). Standard deviations between independent FEP simulations are shown as error bars.

of 9.5 kJ/mol for a simulation time of 20 ns. With a standard deviation of 0.2 kJ/mol (0.4 kJ/mol for 2 ns simulations), the FEP simulations were found to converge well for the ligand in water. As expected, and also found similarly for other simple aldehyde and alcohol compounds (Cramer and Truhlar, 1992), for bombykal, a less favorable solvation free energy than its hydroxyl counterpart

was found, corresponding to its limited ability to form hydrogen bonds with water.

The change in free energy during FEP calculations of bombykol to bombykal within the binding pocket of BmorPBP, ΔG_{FEP}(prot), was 3.9 ± 1.5 kJ/mol (5 ns simulation; 3.8 ± 2.7 for 1 ns simulation). Sampling of the BmorPBP-bombykol and BmorPBP-bombykal conformations during the FEP simulations did not converge well, as reflected by the differences of the free-energy changes obtained for different starting structures. With regard to the time scale of several nanoseconds for hydrogen-bond rupture and formation during the free dynamics of bombykol and bombykal (Figures 2 and 4), longer simulation times would be necessary to sufficiently sample the conformational space of the bound ligand for a more accurate free-energy estimate. Here, however, an accuracy of 1.5 kJ/mol for ΔG_{FEP}(prot) suffices for the comparison of the binding free energies of bombykol and bombykal. It should be noted that the discussed error is restricted to the statistical uncertainty within the accessible time scale of the simulations.

The positive free-energy change during the FEP simulations of the bound state suggests a weaker interaction energy of bombykal to BmorPBP than bombykol. This is consistent with the weaker hydrogen bonding interactions to the binding pocket observed previously for the free bombykal-BmorPBP dynamics. This effect, however, is compensated for by the less favorable solvation of bombykal in water comparing to bombykol. Consequently, according to our FEP calculations, the binding free energies for bombykal and bombykol differ only slightly, by −5.6 ± 1.7 kJ/mol. With a binding free energy of −40.0 kJ/mol for bombykol (Leal et al., 2005b), one obtains −45.6 kJ/mol for bombykal binding (Figure 5C). These experiments thus suggest that both bombykol and bombykal bind to BmorPBP, with equally high affinity.

Our free energy calculations are primarily hampered by the high ligand flexibility, making a sufficient conformational sampling for proper convergence computationally expensive. While FEP has been routinely applied to systems with limited conformational freedom of the ligand with deviations from experimental binding free energies of 4 kJ/mol and less (Reddy and Erion, 2001; van Lipzig et al., 2004; Archontis et al., 2005), it has only recently been successfully used to calculate binding free energies for highly flexible systems like the one investigated here (Guo et al., 2003; Dolenc et al., 2005). Here, the statistical error could be reduced to the order of k_BT by averaging over multiple simulations and extending the simulation time to 5 ns per simulation. We note that, apart from the statistical uncertainty, errors in the free energies also may arise from inaccuracies in the force field of protein and ligand. However, docking studies, being based on different force field parameters, (see below) yielded highly similar results.

Under typical physiological conditions, BmorPBP molecules outnumber the pheromone molecules entering the sensillar antennae to ensure fast and exhaustive transport to the pheromone receptors as required for the high sensitivity of the olfactory system (Klein, 1987). With the small remaining statistical error of a few kJ/mol, our result of a high affinity of BmorPBP for both bombykol and bombykal clearly indicates that under these conditions, BmorPBP efficiently carries both components to the respective receptor. Binding assays and electrophysiology experiments indicated, however, a significant specificity of BmorPBP for bombykol (Pophof, 2004; Oldham et al., 2000, 2001). On the basis of our FEP calculations alone, we can not exclude that a small (few k_BT) albeit significant difference in the binding affinities for bombykol and bombykal of a few k_BT, may lead to preferential binding of one ligand over the other under competitive conditions. This is indeed the case for *Antheraea polyphemus* and *Antheraea pernyi*, in which different PBPs showed up to 5-fold preference for one of the pheromone components (Maida et al., 2000, 2003; Bette et al., 2002; Leal et al., 2005a).

Docking of Bombykol and Bombykal to BmorPBP

To cross-check our findings from MD simulations and free-energy calculations, next, we used AutoDock to perform blind docking of the two ligands to BmorPBP and energy evaluation of the complexes. Even though free-energy calculations from MD simulations can be considered a superior description of the dynamics and energetics of the system, reexamining the results by docking studies as the second approach provides additional confidence. The high number of torsional degrees of freedom (11 for each ligand) represents a challenge to current docking algorithms (Hetenyi and van der Spoel, 2002). The docking algorithm successfully placed the ligands into the central hydrophobic cavity in all 50 docked structures. Within the binding pocket, however, a distinct binding mode could not be identified. Instead, many-fold ligand conformations with various hydrogen bonds to the protein were generated. The minor differences between the docked energies (50 structures within 2–3 k_BT) and the poor clustering of the structures into groups with a ligand rmsd <2 Å (maximal cluster size n = 4 and 5 for bombykol and bombykal, respectively) did not allow proper discrimination among the obtained binding modes. The picture of dissimilar ligand binding modes with similar energies agrees with our previous finding from MD simulations of a flexible ligand in a rigid binding pocket.

The docked conformations are strikingly similar to the crystal structure and the MD ensembles. As an example, the docking results for bombykol and bombykal, respectively, of the cluster with n > 2 and lowest mean docked energy—which also is the largest cluster in both cases—are listed in Table 1. For bombykol, this cluster contains four structures and is ranked third according to the mean docked energy. Likewise, for bombykal, the cluster contains five structures and is ranked third. Figure 6 compares example structures with the crystal structure and selected MD snapshots. The structures share both the intermolecular hydrogen bond to Ser56 (bombykol and bombykal) or Glu98 (bombykol) and the hydrocarbon chain conformation. Given the quite orthogonal approaches of MD simulations and docking, in particular the different force fields, Gromos and AMBER/MMFF for the MD simulations and the docking, respectively, the structural agreement with the experiment and within these two approaches provides further confidence in the obtained conformations and energies.

The lowest docked energy for the bombykol-BmorPBP complex was −43.5 kJ/mol, also in

Table 1. Results of Docking Bombykol and Bombykal to BmorPBP Using AutoDock

	Rank	N	E_{min}	E_{mean}	Hydrogen Bonds
Bombykol	3	4	−43.5	−41.0	Ser56, Glu98
Bombykal	3	5	−42.7	−40.6	Ser56

Only the largest clusters (with population sizes of n = 4 and n = 5, respectively) are shown. E_{min}, minimal energy within cluster; E_{mean}, mean energy of cluster.

remarkable agreement with the experimental binding free energy of −40.0 kJ/mol (Table 1). Our docking simulations yield a lowest docked energy for bombykal-BmorPBP of −42.7 kJ/mol. Taken together, the docking studies, by independently reassessing the findings from FEP simulations, corroborated our conclusion of similar binding affinities of BmorPBP for bombykol and bombykal. Thus, albeit based on a less rigorous molecular description comparing to MD simulations, docking allowed us to conclude with increased certainty that BmorPBP does not discriminate between the two pheromone components.

In Vitro Binding Assays

Binding assays showed that both bombykol and bombykal bound to BmorPBP with similarly high affinity at high pH (Figure 7). We did not observe any significant preference for one ligand or the other in these competitive binding assays. The loss of ligand binding observed at low pH is due to a conformational change that leads to the formation of a C-terminal α helix, which blocks the binding pocket (Horst et al., 2001). These results confirm our findings from free-energy calculations and docking. Thus, BmorPBP does not only strongly bind both pheromone components but also does not function as a selective filter between the two components in competitive situations.

Conclusion

Pheromones for sexual attraction differ within insect species. Excitation by only those pheromone components constituting the pheromone blend of the own species requires highly selective molecular recognition. Is this achieved only by the pheromone receptor or also by perireceptor events? This question was addressed here by characterizing the binding properties and ligand selectivity for the pheromone binding protein of the silk moth, BmorPBP, by means of simulations and binding assays.

Our molecular dynamics simulations depict BmorPBP as a versatile carrier that can accommodate a ligand in various binding modes. An obvious assumption is that it can bind a certain subset of similar ligands, and, in this sense, acts as a prefilter. The discrimination of molecules by BmorPBP was examined here for the natural pheromone components of *B. mori*, bombykol and bombykal. According to our simulation results, bombykal binds to BmorPBP with an affinity similar to bombykol. Also in the affinity measurements, BmorPBP confirmed the absence of any discrimination between bombykol and bombykal. Both ligands bind to the protein with the same high affinity at high pH but showed no binding at low pH.

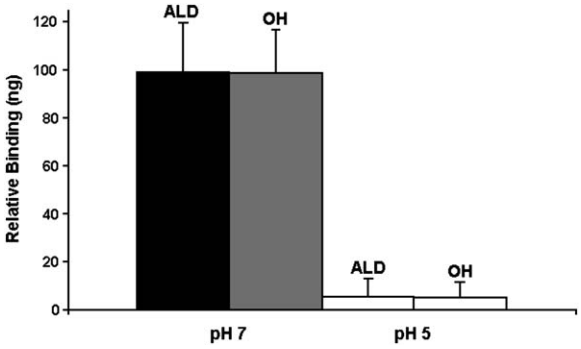

Figure 7. Binding Affinities of Bombykol and Bombykal to the Pheromone-Binding Protein from BmorPBP in a Competitive-Binding Assay

ALD, bombykal; OH, bombykol. Both ligands showed high affinity for the protein at high pH but no affinity at low pH. Results from control experiments with no protein (data not shown) were not significantly different from the results obtained with protein at low pH. Error bars denote standard errors of the mean.

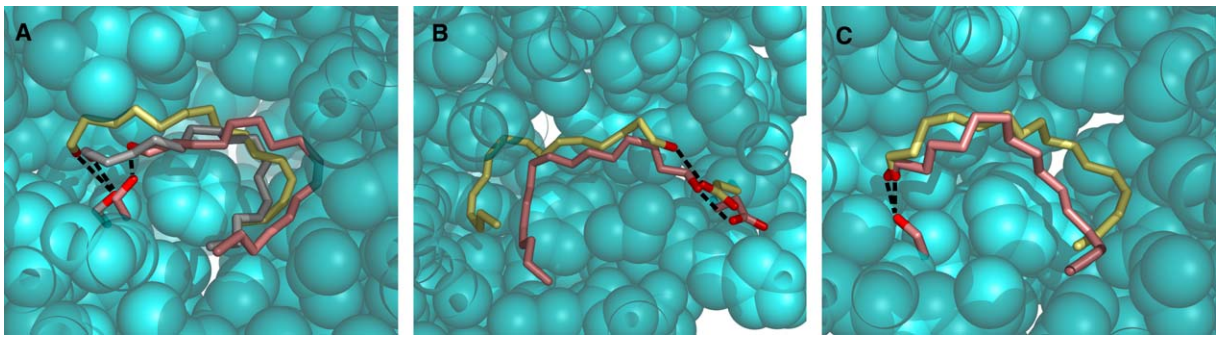

Figure 6. Complex Structures Obtained from Docking, Compared to the Crystal Structure as well as to Structures from MD Simulations

Overlay of structures from docking (yellow, taken from the respective cluster listed in Table 1), with MD structures (pink, 20 ns from MD1, 40 ns from MD2, 35 ns from MD4, respectively) and the crystal structure (gray, 1DQE [Sandler et al., 2000]), after least square fitting of the protein backbone. For clarity, hydrogens are not shown. Only one of the protein structures (1DQE) is shown as cyan spheres. Hydrogen bonds are shown as dashed lines. (A) Bombykol-BmorPBP structures showing a bombykol-Ser56 hydrogen bond. Bombykol and Ser56 are shown as sticks. (B) Bombykol-BmorPBP structures showing a bombykol-Glu98 hydrogen bond. Bombykol and Glu98 are shown as sticks. (C) Bombykal-BmorPBP structures showing a bombykal-Ser56 hydrogen bond. Bombykal and Ser56 are shown as sticks.

The PBPs of *Antheraea polyphemus* and *Bombyx mori* share 67% sequence identity and the main features of the pH-induced conformational switch (Zubkov et al., 2005). In marked contrast to our finding indicating that BmorPBP does not discriminate bombykol and bombykal, the main pheromone-binding protein of *Antheraea polyphemus*, ApolPBP1, differentiates between the three pheromone components with different polar head groups and chain lengths. It prefers the acetate over the aldehyde and the 16-carbon chain over the 14-carbon chain (Leal et al., 2005a). There is structural evidence to suggest Asn53 of ApolPBP1 as the only side chain in the cavity that can act as hydrogen-bond donor for the polar head group of the pheromone molecule (Mohanty et al., 2004). Presumably, the amide-carboxyl interaction is less favorable for the aldehyde comparing to the acetate, to an extent that can not be compensated for by solvation effects. Despite the fact that bombykol and bombykal differ in both the polarity and hydrogen-bonding properties of the polar head, both pheromones bind to BmorPBP with very similar affinity. Our MD simulations suggest that the similar binding affinities arise from several hydrogen-bond interaction partners for both pheromone molecules within the cavity of BmorPBP, as opposed to a single hydrogen bonding in ApolPBP1 pheromone interactions. We therefore suggest that the occurrence of multiple hydrogen-bonding partners at adequate locations within the binding pocket is the major molecular design principle of BmorPBP to accommodate both pheromone components.

Our in silico and experimental data are limited to the interaction between BmorPBP, bombykol, and bombykal. It is known that BmorPBP discriminates other ligands (Wojtasek and Leal, 1999), but we have demonstrated that on the basis of affinity, BmorPBP does not discriminate between the silk moth pheromone and its behavioral antagonist. BmorPBP may act as a prefilter by protecting the receptors from other physiologically irrelevant ligands. It seems, however, that the remarkable selectivity between bombykol and bombykal is determined by molecular interaction between the two semiochemicals and their cognate receptors, which, as the second filter, yield the selectivity required for the excitation by only a single specific pheromone component.

Our results hint at the possibility that, unlike the three PBPs of *Antheraea polyphemus*, BmorPBP is the only PBP known to be expressed by *Bombyx mori* since it can likewise function as a carrier for both pheromone components to their respective receptor. Bombykol and bombykal in this case would share the perireceptor pathway, in contrast to the pathways of the three pheromone components of *Antheraea polyphemus* being largely split up already at the level of the pheromone-PBP interactions. Alternatively, there is a yet unknown PBP from silk moth expressed in the pheromone-detecting sensilla with higher affinity to bombykal and/or bombykal than BmorPBP.

Concerning the physiological function of two layers of filters of PBPs, one may speculate that their interplay not only significantly increases specificity, but also facilitates its fine-tuning and control. For example, to encode the required specificity into the different olfactory proteins across insect species during evolution, two filters can be individually subjected to evolutionary modifications to adjust their affinities. Here, combined simulations and binding assays proved useful to assess the filtering function of the first filter, BmorPBP, for bombykol and bombykal. Extending the calculations to other PBPs will yield a more complete picture of their pheromone discriminative role.

Experimental Procedures

MD Simulations

Protonation states of titratable groups were determined by calculating pK_a values for 1DQE (Sandler et al., 2000) with Whatif (Vriend, 1990) and its interface to DelPhi (Nicholls et al., 1990). None of the five histidine residues of 1DQE was found to be cationic at pH 7. The GROMOS96 force field (van Gunsteren et al., 1996) for the protein and the SPC water model (Berendsen et al., 1981) were used.

Molecular mechanical force field parameters for bombykol (listed in Tables S1 and S2) were determined as follows. Nonbonded and bonded parameters for the saturated part of the aliphatic chain and for the hydroxyl group were adopted from chemically similar fragments, i.e., from serine and threonine, as parametrized in the GROMOS96 force field. For the π-conjugated part of the hydrocarbon chain, Lennard-Jones parameters of the CH-groups were taken from the GROMOS96 force field. Merz-Kollman charges (Singh and Kollman, 1986) were calculated at the B3LYP/6-31G(d) level. They were found to deviate only slightly from zero (−0.17 to −0.16) for the four CH group of the hydrocarbon chain and showed high conformational dependency. Therefore, zero charges were applied except for the polar part of bombykol. Two parameter sets, p1 and p2, have been set up that differ in the parametrization of the conjugated double bonds. Bond lengths and angles of p1 were taken from the crystal structure, 1DQE (Sandler et al., 2000). Force constants of p1 were adopted from quantum mechanical calculations of model systems for the retinal chromophore (Baudry et al., 1997). More specifically, the corresponding bond and angle force constants were adopted from Nina et al. (1995), the dihedral constant for torsion around a double bond from dodecapentene (Said et al., 1984), for torsion around the central bond of the π-system from butadiene (Nina et al., 1993). For set p2, all bonded parameters were taken from the GROMOS96 force field for retinol (van Gunsteren et al., 1996). The dynamics of bombykol and BmorPBP in the bound state were compared for p1 and p2 and found to be sufficiently robust toward the parameters used.

The force-field parameters for bombykal (Tables S3 and S4) were adopted from bombykol set p1 except for the polar head group. The angle including the carbonyl group was set to 125°, as taken from crystallographic studies and Hartree-Fock calculations of acetaldehyde (Ibberson et al., 2000; Gutsev and Adamowicz, 1995). Other parameters, such as the bond length and bond and angle force constants, were adopted from the GROMOS96 force field for carbonyl groups (van Gunsteren et al., 1996).

The protein (PDB entry 1DQE [Sandler et al., 2000]) was solvated in SPC water (Berendsen et al., 1981) molecules in a cubic box of size $7.1 \times 6.7 \times 7.0\ nm^3$. Twelve chloride and 20 sodium ions were added to yield a zero net charge and a physiological ion strength. The resulting simulation system comprised ~32,000 atoms. After 1000 steps of steepest descent energy minimization, the solvent and ions were equilibrated during a 0.5 ns MD simulation with the protein heavy atoms subjected to harmonical constraints with a force constant of $k = 1000\ kJ\ mol^{-1}\ nm^{-2}$. Subsequently, the system was equilibrated for 45 ns. All simulations were carried out with the MD software package GROMACS 3.2.1 (Lindahl et al., 2001) except for the FPMD simulations, for which GROMACS 3.1.4 was used due to technical reasons. All simulations were run in the NpT ensemble. The temperature was kept constant at T = 300 K by coupling to a Berendsen thermostat with a coupling time of $\tau_T = 0.1$ ps (Berendsen et al., 1984). The pressure was kept constant at 1 bar by coupling to a Berendsen barostat with $\tau_p = 1.0$ ps and a compressibility of $4.5\ 10^{-5}\ bar^{-1}$ (Berendsen et al., 1984). All bonds were constrained by using the LINCS algorithm (Hess et al., 1997). An integration step of 2 fs was used. Nonbonded interactions were calculated with a cutoff of 10 Å. Except from free energy perturbation simulations (see

Table 2. Details of MD Simulation Systems for Equilibration

No.	Starting Structure	Time	Remarks
MD1	1DQE	45 ns	bombykol set p1, for REMD and ED
MD2	1DQE	45 ns	bombykol set p2
MD3	snapshot from MD1, bombykol as hydrogen bond acceptor	60 ns	bombykal
MD4	snapshot from MD1, bombykol as hydrogen bond donor	60 ns	bombykal

below), long-range electrostatic interactions were calculated by Particle-Mesh Ewald summation (Darden et al., 1993) with a grid spacing of 0.12 nm and cubic interpolation.

Four simulation systems were setup, as detailed in Table 2. All four systems were subjected to the same simulation protocol as described above. Simulation time lengths comprising production and equilibration of the system are given in Table 2. All protein structures were plotted with Pymol (DeLano, 2001).

Free-Energy Calculations

The difference between the binding free energies of bombykal (al) and bombykol (ol), $\Delta\Delta G_b = \Delta G_{b,al} - \Delta G_{b,ol}$, was calculated from the free energies ΔG_{FEP}(prot) and ΔG_{FEP}(aq), which correspond to the free-energy difference between the two ligands in aqueous solution and in the protein complex, respectively. The underlying thermodynamic cycle is shown in Figure 5A. ΔG_{FEP}(prot) was obtained by carrying out free energy perturbation (FEP) simulations along the (unphysical) pathway from bombykol to the bombykal when bound to the protein, "mutating" the ligand from bombykol to bombykal (Bash et al., 1987; Simonson et al., 2002). ΔG_{FEP}(aq) was obtained similarly, but for the ligand in solution. The "mutation" was done by interpolating between the two ligand topologies as follows. Within the time course of one FEP simulation, the scaling factor λ was gradually changed from 0 to 1 with an identical increase of λ at each MD step. The bombykol- and bombykal-bonded potential energies were linearly scaled by λ, yielding a total bonded potential V_b,

$$V_b = (1 - \lambda)V_{b,ol} + \lambda V_{b,al}. \quad (1)$$

The hydrogen atom of the bombykol hydroxyl group was mutated to a dummy atom; i.e., its charges and Lennard-Jones parameters were changed to zero. The appearance or disappearance of this atom close to $\lambda = 0$ and $\lambda = 1$ gave rise to singularities of the nonbonded potentials when interpolated linearly. To remove this known problem, nonbonded interactions were calculated with soft-core potentials (Nilges et al., 1988; Beutler et al., 1994). The soft-core parameter α, which controls the height of the potential at zero distance, was set to 1.51 (Schäfer et al., 1999). The interaction radius σ was chosen as the Lennard-Jones parameters, with $(C_{12}/C_6)^{1/6}$, for $C_{12}, C_6 \neq 0$, otherwise $\sigma = 0.3$.

Docking

The AutoDock program (Goodsell et al., 1996; Morris et al., 1998) using a genetic search algorithm and an empirical free-energy function was used for the flexible docking of bombykol and bombykal to BmorPBP without predefining the binding site ("blind docking"). For the protein, the crystallographic structure 1DQE (Sandler et al., 2000) was used. Crystallographic water was removed, and polar hydrogen bonds were added to the protein and the hydroxyl group of bombykol. Gasteiger charges were used for the ligand (Gasteiger and Marsili, 1978). All torsions were released except those around the conjugated double bonds, resulting in eleven degrees of freedom. The AMBER/MMFF force field (Cornell et al., 1995; Halgren, 1996) as supplied with the AutoDock program was applied. Grid maps with 0.374 Å spacing were calculated for the whole protein.

The genetic algorithm was applied with default parameters starting from random positions and orientations of the ligands. The number of trials was set to 200, with $3 \cdot 10^6$ energy evaluations and 54,000 generations. The population in the genetic algorithm was 50. The resulting docked structures were clustered with a 2 Å rmsd tolerance.

Binding Assays

Recombinant BmorPBP was produced and purified as previously described (Wojtasek and Leal, 1999). Bombykol and bombykal, purchased from Plant Research International (Wageningen, The Netherlands), were dissolved in UV grade ethanol. Working solutions (3.2 mM for each ligand) were prepared, with the 1:1 ratio being adjusted by gas chromatography. BmorPBP solutions (50 μl; 6.2 μM) either in ammonium acetate (100 mM [pH 7]) or sodium acetate (100 mM [pH 5]) were prepared in glass inserts deactivated by Silcote CL7 treatment (Kimble Chromatography, Vineland, NJ). One microliter of a bombykol+bombykal solution (3.2 mM for each ligand) was transferred to each reaction vial. The reaction mixture was shaken at 100 rpm and at 25°C ± 2°C for 1 hr. For separation of the bound and free ligands, the reaction mixtures were transferred individually to washed Microcons YM-10 (Millipore) and centrifuged (12,000 × g, 4°C ± 2°C) for 10 min. A second filtration (15 min) was done after adding 50 μl of 20 mM buffer with the same pH of the reaction.

The retentate from each centrifugal device was then transferred to a 100 μl V-vial (Wheaton, Millville, NJ) along with 20 μl of internal standard (eicosyl acetate, Fuji Flavor, Co., Tokyo, Japan) in hexane. Two washes of the centrifugal device (10 and 5 μl, respectively) with buffer were pooled in the V-vial and treated with 1 M sodium formate (50 μl) to release the bound ligand. Then, 20 μl of internal standard (eicosyl acetate, Fuji Flavor, Co., Tokyo, Japan) in hexane was added, and the vials were capped, vortexed for 30 s, and then centrifuged (2,500 × g, 4°C ± 2°C) for 7 min. The hexane fraction (upper layer) was analyzed by gas chromatography for quantification. Binding activity was determined by the amount of bound ligand detected (n = 10 trials).

Supplemental Data

Supplemental Data include the bombykol and bombykal force fields and are available online at http://www.structure.org/cgi/content/full/14/10/1577/DC1/.

Acknowledgments

We thank Karl-Ernst Kaissling for stimulating discussions and for carefully reading the manuscript and Matthias Müller for help with AutoDock. This work was supported by Volkswagen Foundation grants I/78 420 and I/80 585 (to H.G.) and a PhD scholarship of the Boehringer Ingelheim Fonds (to F.G.). Work in Davis was supported by the National Research Initiative of the U.S. Department of Agriculture (USDA-CSREES, 2003-13648).

Received: June 19, 2006
Revised: July 25, 2006
Accepted: August 2, 2006
Published: October 10, 2006

References

Archontis, G., Watson, K.A., Xie, Q., Andreou, G., Chrysina, E.D., Zographos, S.E., Oikonomakos, N.G., and Karplus, M. (2005). Glycogen phosphorylase inhibitors: a free energy perturbation analysis of glucopyranose spirohydantoin analogues. Proteins *61*, 984–998.

Bash, P.A., Singh, U.C., Brown, F.K., Langridge, R., and Kollman, P.A. (1987). Calculation of the relative change in binding free-energy of a protein-inhibitor complex. Science *235*, 574–576.

Baudry, J., Crouzy, S., Roux, B., and Smith, J.C. (1997). Quantum chemical and free energy simulation analysis of retinal conformational energetics. J. Chem. Inf. Comput. Sci. *37*, 1018–1024.

Berendsen, H.J.C., Postma, J.P.M., van Gunsteren, W.F., and Hermans, J. (1981). Interaction Model for Water in Relation to Protein Hydration (Dordrecht, The Netherlands: D. Reidel Publishing Company).

Berendsen, H.J.C., Postma, J.P.M., van Gunsteren, W.F., Nola, A.D., and Haak, J.R. (1984). Molecular dynamics with coupling to an external bath. J. Chem. Phys. *81*, 3684–3690.

Bette, S., Breer, H., and Krieger, J. (2002). Probing a pheromone binding protein of the silkmoth *Antheraea polyphemus* by endogenous tryptophan fluorescence. Insect Biochem. Mol. Biol. *32*, 241–246.

Beutler, T.C., Mark, A.E., Vanschaik, R.C., Gerber, P.R., and van Gunsteren, W.F. (1994). Avoiding singularities and numerical instabilities in free-energy calculations based on molecular simulations. Chem. Phys. Lett. *222*, 529–539.

Campanacci, V., Krieger, J., Bette, S., Sturgis, J.N., Lartigue, A., Cambillau, C., Breer, H., and Tegoni, M. (2001). Revisiting the specificity of *Mamestra brassicae* and *Antheraea polyphemus* pheromone-binding proteins with a fluorescence binding assay. J. Biol. Chem. *276*, 20078–20084.

Cornell, W.D., Cieplak, P., Bayly, C.I., Gould, I.R., Merz, K.M., Ferguson, D.M., Spellmeyer, D.C., Fox, T., Caldwell, J.W., and Kollman, P.A. (1995). A second generation force field for the simulation of proteins, nucleic acids, and organic molecules. J. Am. Chem. Soc. *117*, 5179–5197.

Cramer, C.J., and Truhlar, D.G. (1992). An SCF solvation model for the hydrophobic effect and absolute free energies of aqueous solvation. Science *256*, 213–217.

Darden, T., York, D., and Pedersen, L. (1993). Particle mesh Ewald—an Nlog(N) method for Ewald sums in large systems. J. Chem. Phys. *98*, 10089–10092.

DeLano, W.L. (2001). PyMOL Manual (San Carlos, CA: DeLano Scientific).

Dolenc, J., Oostenbrink, C., Koller, J., and van Gunsteren, W.F. (2005). Molecular dynamics simulations and free energy calculations of netropsin and distamycin binding to an AAAAA DNA binding site. Nucleic Acids Res. *33*, 725–733.

Du, G.H., and Prestwich, G.D. (1995). Protein-structure encodes the ligand-binding specificity in pheromone binding-proteins. Biochemistry *34*, 8726–8732.

Gasteiger, J., and Marsili, M. (1978). A new model for calculating atomic charges in molecules. Tetrahedron Lett. *34*, 3181–3184.

Goodsell, D.S., Morris, G.M., and Olson, A.J. (1996). Automated docking of flexible ligands: applications of AutoDock. J. Mol. Recognit. *9*, 1–5.

Guo, Z.Y., Durkin, J., Fischmann, T., Ingram, R., Prongay, A., Zhang, R.M., and Madison, V. (2003). Application of the lambda-dynamics method to evaluate the relative binding free energies of inhibitors to HCV protease. J. Med. Chem. *46*, 5360–5364.

Gutsev, G.L., and Adamowicz, L. (1995). Electronic and geometrical structure of dipole-bound anions formed by polar-molecules. J. Phys. Chem. *99*, 13412–13421.

Halgren, T.A. (1996). Merck molecular force field. 1. Basis, form, scope, parameterization, and performance of MMFF94. J. Comput. Chem. *17*, 490–519.

Hekmat-Scafe, D.S., Steinbrecht, R.A., and Carlson, J.R. (1997). Coexpression of two odorant-binding protein homologs in *Drosophila*: implications for olfactory coding. J. Neurosci. *17*, 1616–1624.

Hess, B., Bekker, H., Berendsen, H.J.C., and Fraaije, J.G.E.M. (1997). LINCS: a linear constraint solver for molecular simulations. J. Comput. Chem. *18*, 1463–1472.

Hetenyi, C., and van der Spoel, D. (2002). Efficient docking of peptides to proteins without prior knowledge of the binding site. Protein Sci. *11*, 1729–1737.

Horst, R., Damberger, F., Luginbuhl, P., Guntert, P., Peng, G., Nikonova, L., Leal, W.S., and Wuthrich, K. (2001). NMR structure reveals intramolecular regulation mechanism for pheromone binding and release. Proc. Natl. Acad. Sci. USA *98*, 14374–14379.

Ibberson, R.M., Yamamuro, O., and Matsuo, T. (2000). Crystal structures and phase behaviour of acetaldehyde-d(4): a study by high-resolution neutron powder diffraction and calorimetry. J. Mol. Struct. *520*, 265–272.

Kaissling, K.E. (2001). Olfactory perireceptor and receptor events in moths: A kinetic model. Chem. Senses *26*, 125–150.

Kaissling, K.E., and Kasang, G. (1978). New pheromone of silkworm moth *Bombyx mori*—sensory pathway and behavioral effect. Naturwissenschaften *65*, 382–384.

Kaissling, K.-E., Klein, U., de Kramer, J., Keil, T., Kanaujia, S., and Hemberger, J. (1985). Insect olfactory cells: electrophysiological and biochemical studies. In Molecular Basis of Nerve Activity, J.P. Changeux, F. Hucho, A. Maelicke, and E. Neuman, eds. (Berlin: de Gruyter), pp. 173–183.

Klein, U. (1987). Sensillum-lymph proteins from antennal olfactory hairs of the moth *Antheraea polyphemus* (saturniidae). Insect Biochem. *17*, 1193–1204.

Klusak, V., Havlas, Z., Rulisek, L., Vondrasek, J., and Svatos, A. (2003). Sexual attraction in the silkworm moth: nature of binding of bombykol in pheromone binding protein—an ab initio study. Chem. Biol. *10*, 331–340.

Krieger, J., and Breer, H. (1999). Olfactory reception in invertebrates. Science *286*, 720–723.

Leal, W.S. (2005). Pheromone reception. Top. Curr. Chem. *240*, 1–36.

Leal, W.S., Chen, A.M., and Erickson, M.L. (2005a). Selective and pH-dependent binding of a moth pheromone to a pheromone-binding protein. J. Chem. Ecol. *31*, 2493–2499.

Leal, W.S., Chen, A.M., Ishida, Y., Chiang, V.P., Erickson, M.L., Morgan, T.I., and Tsuruda, J.M. (2005b). Kinetics and molecular properties of pheromone binding and release. Proc. Natl. Acad. Sci. USA *102*, 5386–5391.

Lindahl, E., Hess, B., and van der Spoel, D. (2001). GROMACS 3.0: a package for molecular simulation and trajectory analysis. J. Mol. Model. (Online) *7*, 306–317.

Maibeche-Coisne, M., Sobrio, F., Delaunay, T., Lettere, M., Dubroca, J., Jacquin-Joly, E., and Nagnan-Le Meillour, P. (1997). Pheromone binding proteins of the moth *Mamestra brassicae*: specificity of ligand binding. Insect Biochem. Mol. Biol. *27*, 213–221.

Maida, R., Proebstl, T., and Laue, M. (1997). Heterogeneity of odorant-binding proteins in the antennae of *Bombyx mori*. Chem. Senses *22*, 503–515.

Maida, R., Krieger, J., Gebauer, T., Lange, U., and Ziegelberger, G. (2000). Three pheromone-binding proteins in olfactory sensilla of the two silkmoth species *Antheraea polyphemus* and *Antheraea pernyi*. Eur. J. Biochem. *267*, 2899–2908.

Maida, R., Ziegelberger, G., and Kaissling, K.E. (2003). Ligand binding to six recombinant pheromone-binding proteins of *Antheraea polyphemus* and *Antheraea pernyi*. J. Comp. Physiol. [B] *173*, 565–573.

Mohanty, S., Zubkov, S., and Gronenborn, A.M. (2004). The solution NMR structure of *Antheraea polyphemus* PBP provides new insight into pheromone recognition by pheromone-binding proteins. J. Mol. Biol. *337*, 443–451.

Morris, G.M., Goodsell, D.S., Halliday, R.S., Huey, R., Hart, W.E., Belew, R.K., and Olson, A.J. (1998). Automated docking using a Lamarckian genetic algorithm and an empirical binding free energy function. J. Comput. Chem. *19*, 1639–1662.

Nakagawa, T., Sakurai, T., Nishioka, T., and Touhara, K. (2005). Insect sex-pheromone signals mediated by specific combinations of olfactory receptors. Science *307*, 1638–1642.

Nicholls, A., Sharp, K.A., and Honig, B. (1990). DelPhi V3.0 (New York: Columbia University).

Nilges, M., Clore, G.M., and Gronenborn, A.M. (1988). Determination of three-dimensional structures of proteins from interproton distance data by dynamical simulated annealing from a random array of atoms. Circumventing problems associated with folding. FEBS Lett. *239*, 129–136.

Nina, M., Smith, J.C., and Roux, B. (1993). Ab-initio quantum-chemical analysis of schiff-base water interactions in bacteriorhodopsin. J. Mol. Struct. *105*, 231–245.

Nina, M., Roux, B., and Smith, J.C. (1995). Functional interactions in bacteriorhodopsin—a theoretical analysis of retinal hydrogen bonding with water. Biophys. J. *68*, 25–39.

Oldham, N.J., Krieger, J., Breer, H., Fischedick, A., Hoskovec, M., and Svatos, A. (2000). Analysis of the silkworm moth pheromone binding protein-pheromone complex by electrospray-ionization mass spectrometry. Angew. Chem. Int. Ed. Engl. *39*, 4341–4343.

Oldham, N.J., Krieger, J., Breer, H., and Svatos, A. (2001). Detection and removal of an artefact fatty acid from the binding site of recombinant *Bombyx mori* pheromone-binding protein. Chem. Senses *26*, 529–531.

Plettner, E., Lazar, J., Prestwich, E.G., and Prestwich, G.D. (2000). Discrimination of pheromone enantiomers by two pheromone binding proteins from the gypsy moth *Lymantria dispar*. Biochemistry *39*, 8953–8962.

Pophof, B. (2002). Moth pheromone binding proteins contribute to the excitation of olfactory receptor cells. Naturwissenschaften *89*, 515–518.

Pophof, B. (2004). Pheromone-binding proteins contribute to the activation of olfactory receptor neurons in the silkmoths *Antheraea polyphemus* and *Bombyx mori*. Chem. Senses *29*, 117–125.

Prestwich, G.D., Du, G.H., and Laforest, S. (1995). How is pheromone specificity encoded in proteins. Chem. Senses *20*, 461–469.

Reddy, M.R., and Erion, M.D. (2001). Calculation of relative binding free energy differences for fructose 1,6-bisphosphatase inhibitors using the thermodynamic cycle perturbation approach. J. Am. Chem. Soc. *123*, 6246–6252.

Rutzler, M., and Zwiebel, L.J. (2005). Molecular biology of insect olfaction: recent progress and conceptual models. J. Comp. Physiol. A Neuroethol. Sens. Neural Behav. Physiol. *191*, 777–790.

Said, M., Maynau, D., Malrieu, J.P., and García Bach, M.A. (1984). A nonempirical Heisenberg Hamiltonian for the study of conjugated hydrocarbons. Ground-state conformational studies. J. Am. Chem. Soc. *106*, 571–579.

Sakurai, T., Nakagawa, T., Mitsuno, H., Mori, H., Endo, Y., Tanoue, S., Yasukochi, Y., Touhara, K., and Nishioka, T. (2004). Identification and functional characterization of a sex pheromone receptor in the silkmoth *Bombyx mori*. Proc. Natl. Acad. Sci. USA *101*, 16653–16658.

Sandler, B.H., Nikonova, L., Leal, W.S., and Clardy, J. (2000). Sexual attraction in the silkworm moth: structure of the pheromone-binding-protein-bombykol complex. Chem. Biol. *7*, 143–151.

Schäfer, H., van Gunsteren, W.F., and Mark, A.E. (1999). Estimating relative free energies from a single ensemble: hydration free energies. J. Comput. Chem. *20*, 1604–1617.

Simonson, T., Archontis, G., and Karplus, M. (2002). Free energy simulations come of age: protein-ligand recognition. Acc. Chem. Res. *35*, 430–437.

Singh, U.C., and Kollman, P.A. (1986). A combined abinitio quantum mechanical and molecular mechanical method for carrying out simulations on complex molecular systems: applications to the CH3Cl + Cl^- exchange reaction and gas phase protonation of polyethers. J. Comput. Chem. *7*, 718–730.

Steinbrecht, R.A. (1996). Are odorant-binding proteins involved in odorant discrimination? Chem. Senses *21*, 719–727.

Steinbrecht, R.A., Laue, M., and Ziegelberger, G. (1995). Immunolocalization of insect odorant-binding proteins—a comparative-study. Chem. Senses *20*, 109–110.

van Gunsteren, W.F., Billeter, S.R., Eising, A.A., Hünenberger, P.H., Krüger, P., Mark, A.E., Scott, W.R.P., and Tironi, I.G. (1996). Biomolecular Simulation: The GROMOS96 Manual and User Guide (Zürich, Switzerland: Vdf Hochschulverlag AG an der ETH Zürich).

van Lipzig, M.M.H., ter Laak, A.M., Jongejan, A., Vermeulen, N.P.E., Wamelink, M., Geerke, D., and Meerman, J.H.N. (2004). Prediction of ligand binding affinity and orientation of xenoestrogens to the estrogen receptor by molecular dynamics simulations and the linear interaction energy method. J. Med. Chem. *47*, 1018–1030.

Vogt, R.G., and Riddiford, L.M. (1981). Pheromone binding inactivation by moth antennae. Nature *293*, 161–163.

Vriend, G. (1990). WHAT IF: a molecular modelling and drug design program. J. Mol. Graph. *8*, 52–56.

Wlodek, S.T., Clark, T.W., Scott, L.R., and McCammon, J.A. (1997). Molecular dynamics of acetylcholinesterase dimer complexed with tacrine. J. Am. Chem. Soc. *119*, 9513–9522.

Wojtasek, H., and Leal, W.S. (1999). Conformational change in the pheromone-binding protein from *Bombyx mori* induced by pH and by interaction with membranes. J. Biol. Chem. *274*, 30950–30956.

Zubkov, S., Gronenborn, A.M., Byeon, I.J., and Mohanty, S. (2005). Structural consequences of the pH-induced conformational switch in a. polyphemus pheromone-binding protein: mechanisms of ligand release. J. Mol. Biol. *354*, 1081–1090.